https://doi.org/10.5194/egusphere-2026-3646
Preprint. Discussion started: 13 July 2026

Determination of water diffusion coefficients in aerosols based on characteristic time analysis

Shuqi Guo[1], Chengyi Fan[1], Chunsheng Zhao[1]

[1]Department of Atmospheric and Oceanic Sciences, School of Physics, Peking University, Beijing, 100871, China

Correspondence to: Chunsheng Zhao (zcs@pku.edu.cn)

Abstract. The water diffusion coefficient in atmospheric particles is a key parameter characterising particle-phase water transport and is essential for understanding aerosol phase state, phase transitions, and multiphase chemical processes. In this study, we develop a characteristic-time-based method for directly measuring the water diffusion coefficient in an individual droplet. The progress of water diffusion is represented by the relative abundance of H_2O and D_2O within the droplet, which is retrieved from Raman spectra and quantified here as the D_2O fraction. The characteristic time is derived as the time at which the measured D_2O fraction reaches the value predicted by the aqueous-phase diffusion model. Since the characteristic time derived from this model depends only on the water diffusion coefficient and droplet radius, the water diffusion coefficient can be calculated directly from the measured characteristic time and droplet radius. Using this method, water diffusion coefficients in sucrose droplets at 30-45% RH were determined to be 1×10^{-16} to 1×10^{-14} m^2s^{-1}. The water diffusion coefficient showed a clear RH dependence, with lower coefficients observed at lower RH. These results are consistent with previous experimental measurements, supporting the reliability of our method. A key advantage of this method is that it does not require tracking the complete H_2O/D_2O exchange process, as measurements are only needed until the characteristic time, thereby shortening the experimental observation time and making the method particularly suitable for diffusion measurements in highly viscous aerosol particles. This method applies to both spherical droplets and non-spherical diffusion systems, which allows it to be adapted to different experimental platforms. It therefore provides a basis for understanding mass transport in aerosols and related atmospheric chemical processes.

1 Introduction

Atmospheric aerosol interactions with environmental water vapour are involved in key processes, including aerosol hygroscopic growth, evaporation, multiphase chemistry, and the formation of cloud droplets and precipitation (Mason, 2010). Related studies have long assumed that water molecules within aerosol particles diffuse sufficiently rapidly to complete internal mass transport, allowing the particles to equilibrate quickly with changes in ambient relative humidity (RH) (Seinfeld and Pandis, 1998; Semeniuk and Dastoor, 2020). However, increasing evidence indicates that atmospheric aerosols are not always present as homogeneous liquids, but may exist as highly viscous semisolids or even glassy states under specific environmental conditions (Zobrist et al., 2008; Shiraiwa et al., 2017; Reid et al., 2018). Under these conditions,

https://doi.org/10.5194/egusphere-2026-3646
Preprint. Discussion started: 13 July 2026

molecular diffusion within the particles can be substantially hindered, so that their response to changes in ambient humidity is no longer instantaneous but exhibits pronounced kinetic delays and non-equilibrium behaviour. This can in turn modify particle size distributions (Zaveri et al., 2018), gas–particle partitioning (Shiraiwa and Seinfeld, 2012), multiphase chemical kinetics (Zhou et al., 2013; Slade and Knopf, 2014; Rasool et al., 2023), and ice nucleation mechanisms (Wilson et al., 2012), ultimately exerting significant effects on human health, air quality, and global climate (Reid et al., 2018; Gou et al., 2025).

The water diffusion coefficient (D_w) in aerosol particles determines the timescale of internal water redistribution and is therefore a key parameter for assessing the extent of mass-transfer limitations. Water diffusion coefficients have commonly been estimated indirectly from particle viscosity through the Stokes–Einstein relation (Evoy et al., 2019). Although a series of methods has been developed to measure aerosol viscosity, including poke-flow, shape relaxation, particle rebound, fluorescence lifetime imaging (FLIM), and microscopy-based techniques (Renbaum-Wolff et al., 2013; Power et al., 2013; Virtanen et al., 2010; Hosny et al., 2013, 2016; Kiland et al., 2022; Madawala et al., 2023), previous studies have shown that the Stokes–Einstein relation can break down in highly viscous systems, making it difficult to accurately predict the water diffusion coefficient under such conditions (Price et al., 2014; Song et al., 2020).

Recently, single-particle trapping combined with spectroscopic tracing has enabled direct, in situ measurements of water diffusion in highly viscous droplets. Zobrist et al. used the electrodynamic balance (EDB) with stepwise changes in relative humidity to establish a mass-transfer model and determine water diffusion coefficients in sucrose droplets (Zobrist et al., 2011). Price et al. subsequently developed a Raman isotope tracer method based on monitoring H_2O/D_2O exchange, which enabled direct retrieval of water diffusion behaviour in highly viscous solutions and quantitative characterisation of the dependence of the water diffusion coefficient on RH (Price et al., 2014). This isotope tracer method was later applied to both optical tweezer systems and EDB (Davies and Wilson, 2016; Nadler et al., 2019), extending direct measurements of water diffusion coefficients to suspended single droplets. These studies provide a novel experimental foundation for elucidating the mechanisms of internal mass transfer limitations within droplets and for improving parameterisations in atmospheric models. Compared with mass transfer methods that determine the water diffusion coefficient from step changes in RH, the Raman isotope tracer method is performed under constant RH conditions and thus avoids the stagewise changes in droplet radius and composition induced by hygroscopic growth or evaporation, making the diffusion model easier to formulate and solve (Price et al., 2014; Davies and Wilson, 2016). However, in systems with slow water diffusion, the method still faces practical limitations due to the need for long observation time, a problem that is particularly evident in measurements based on solution disks and EDB. The relatively large sample or droplet size in these two experimental systems substantially prolongs the time required for complete H_2O/D_2O exchange. For solution disks, when the water diffusion coefficient is on the order of 10^{-16}, the measurement takes approximately 8 days (Price et al., 2014). Similarly, EDB studies have indicated that, for sucrose droplets at RH below 25%, isotope tracer measurements of D_w become impractical because of prohibitively long diffusion timescales (Nadler et al., 2019). Consequently, when the water diffusion coefficient is exceptionally low, isotope exchange experiments often need to run continuously for several days or longer. This imposes stringent requirements on stable temperature and humidity control, as well as on the long-term operational stability of the measurement systems.

https://doi.org/10.5194/egusphere-2026-3646
Preprint. Discussion started: 13 July 2026

The combination of optical tweezers and Raman isotope tracer offers several advantages for measuring the water diffusion coefficient, including relatively simple modelling, short equilibration time, and the ability to probe supersaturated states (Davies and Wilson, 2016). Using an optical tweezer system, this study develops a characteristic-time-based method for retrieving water diffusion coefficients in droplets and applies it to sucrose droplets at different relative humidities. The measured results are consistent with previous studies. Compared with the conventional Raman isotope tracer method, this approach does not require monitoring the full isotope exchange process and therefore reduces the experimental observation time. The method is also potentially applicable to non-spherical diffusion systems, providing a methodological reference for future direct measurements of water diffusion coefficients in highly viscous systems across different experimental platforms.

2 Optical tweezer experimental system and measurement of isotopic exchange in droplets

2.1 Optical trapping system and sample preparation

The optical tweezers system used in this work builds on the setup reported by previous studies (Qiu et al., 2024; Fan et al., 2025), and only the key experimental features are summarized here (Fig. 1) . In this study, the gas-flow configuration was modified to include three separate flow paths for dry nitrogen (N_2), H_2O-humidified N_2, and D_2O-humidified N_2, allowing RH control and switching between H_2O and D_2O environments. A 532-nm laser beam with an initial power of 200 mW was expanded and focused before being directed vertically upward into the sample chamber. A high-gradient optical field was generated near the focal region, enabling stable trapping of individual droplets.

The experimental solution was prepared by dissolving sucrose (99.5% AR; Shanghai Hong Bo Technology Co., Ltd.) in ultrapure water (18 MΩ·cm; SIMGEN; Hangzhou SIMGEN Biotechnology Co., Ltd.). The prepared solution was then aerosolised using a medical ultrasonic nebuliser (Yuyue 402AI model) to generate micrometre-sized droplets, which were then introduced into the sample chamber. An individual droplet could be captured and stably levitated by the optical trap for subsequent Raman spectroscopic analysis.

https://doi.org/10.5194/egusphere-2026-3646
Preprint. Discussion started: 13 July 2026

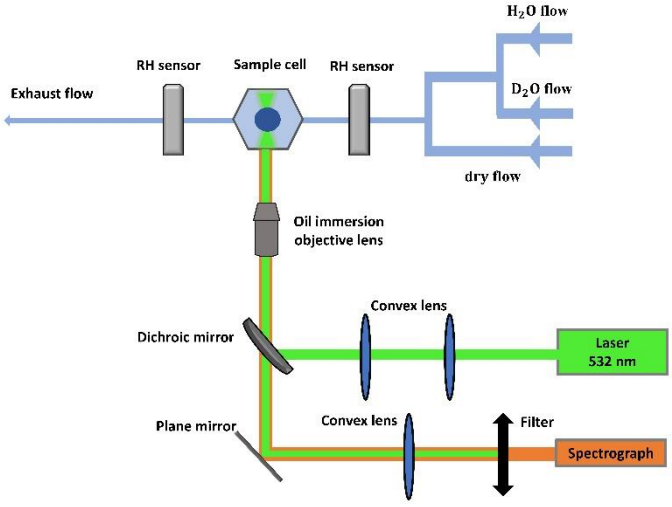

Figure 1: Schematic diagram of the optical tweezer experimental system.

2.2 H_2O/D_2O exchange and experimental environmental control

The experimental principle and procedure of the Raman isotope tracer method have been comprehensively described in previous studies (Price et al., 2014). In each experiment, a single sucrose droplet was first trapped by the optical tweezers in an H_2O vapour environment at a preset relative humidity. After the droplet had reached hygroscopic equilibrium with the surrounding atmosphere, the H_2O vapour flow was terminated and replaced with a D_2O vapour flow at the same RH, thereby switching the gas phase environment surrounding the droplet from H_2O vapour to D_2O vapour. During this process, Raman spectroscopy was used to monitor the progressive replacement of H_2O by D_2O within the droplet, thereby allowing the water diffusion coefficient in the droplet to be determined.

The experimental temperature was maintained at 25±1°C using an air conditioning system. The relative humidity within the experimental setup was controlled by adjusting the flow rate ratio between the dry and humidified nitrogen gas streams. The gas delivery system consisted of three flow paths: a dry N_2 stream, an H_2O-humidified N_2 stream, and a D_2O-humidified N_2 stream. The flow rates of these three streams were independently regulated by their respective mass flow controllers (MFCs, Dmass, DFC10-1/4-N2-3000SCCM-B01) to establish the desired RH conditions. Two temperature – humidity probes (Rotronic, HC2A-S) were installed upstream and downstream of the sample chamber to continuously record the conditions of the inflowing and outflowing gas, allowing for monitoring of the stability of the chamber environment.

In each experiment, one H_2O/D_2O switching process was performed under each preset RH condition. It should be noted that the RH value reported by the temperature-humidity probe is generally defined as the ratio of the actual vapour partial pressure to the saturation vapour pressure of pure H_2O at the present temperature. By contrast, in a D_2O vapour environment, the actual RH should be defined as the ratio of the actual vapour partial pressure to the saturation vapour pressure of pure D_2O. Therefore, after switching to the D_2O vapour, the probe reading must be calibrated as follows:

https://doi.org/10.5194/egusphere-2026-3646
Preprint. Discussion started: 13 July 2026

$$RH_{real} = RH_{measure} \times \frac{e_s(H_2O)}{e_s(D_2O)}, \quad (1)$$

where $RH_{measure}$ is the RH value reported by the temperature-humidity probe, and RH_{real} is the actual RH of the D_2O vapour environment. The ratio of the saturation vapour pressure of pure H_2O to that of pure D_2O can be determined using the empirical relationship reported by Narten (1964). The parameterisation adopted in this study is as follows:

$$ln[\frac{e_s(H_2O)}{e_s(D_2O)}] = -0.0705984 + \frac{21.0469}{T - 197.397}, \quad (2)$$

where T is the temperature in kelvin.

2.3 Determination of the D_2O fraction in an individual droplet from Raman spectroscopy

The Raman spectra of the trapped droplets were acquired using a Raman spectrometer (Zolix Omniλ-300i, 1200 grooves mm^{-1}) coupled to a CCD camera (Andor Solis 256, 1024 × 256 pixels), with spectra recorded at 1 frame per second. The resulting Raman signals were used to analyse both droplet size and composition. Droplet radius was retrieved from the whispering gallery modes (WGMs) in the spectra in combination with Mie scattering theory (Reid et al., 2007).

Spontaneous Raman spectra of the droplet were collected simultaneously in the O – D and O – H stretching regions. The temporal evolution of these two characteristic bands reflects the changing extent of D_2O substitution within the droplet, thereby enabling the diffusion of D_2O in the droplet to be tracked. Figure 2 shows the Raman spectra of a sucrose droplet at RH=35% before D_2O exchange (a), during the exchange process (b), and after the exchange was completed (c). As the H_2O/D_2O exchange proceeded, the O–D band gradually increased, whereas the O–H band gradually decreased. The fraction of D_2O within the droplet can be expressed by Eq. (3), which represents the relative abundances of the O–D and O–H band within the sampled region (Price et al., 2014):

$$\Phi_{D_2O} = \frac{A_{D_2O}}{A_{D_2O} + \frac{1}{\sqrt{2}}A_{H_2O}}, \quad (3)$$

Where Φ_{D_2O} denotes the D_2O fraction, A_{D_2O} is the integrated area of the O–D band, A_{H_2O} is the integrated area of the O–H band, and $\frac{1}{\sqrt{2}}$ is a correction factor arising from the difference in integrated Raman intensities between the O–D and O–H stretching bands (Price et al., 2014). In optical tweezers experiments, the Raman signal is more representative of the radially averaged composition within the probed region than of the volume-averaged composition of the entire droplet, because the beam cross section is typically smaller than the droplet diameter (Davies and Wilson, 2016). Therefore, Φ_{D_2O} is more appropriately interpreted as characterising the extent of D_2O exchange in terms of the radial average within the droplet, rather than the volume averaged fraction of the whole droplet.

To obtain A_{D_2O} and A_{H_2O}, the Raman spectra over the range 2200-3700 cm^{-1} were fitted with six Gaussian peaks and a constant baseline. This spectral region includes the O–D stretching band of D_2O, the O–H stretching band of H_2O, and the C–H stretching band of sucrose. Specifically, one Gaussian peak was used to fit the O–D band, three Gaussian peaks were

https://doi.org/10.5194/egusphere-2026-3646
Preprint. Discussion started: 13 July 2026

used for the C–H band, and two Gaussian peaks were used for the O–H band. A constant baseline was included to account for the instrumental background signal. The six Gaussian peaks and the overall fit are shown in Fig. 2.

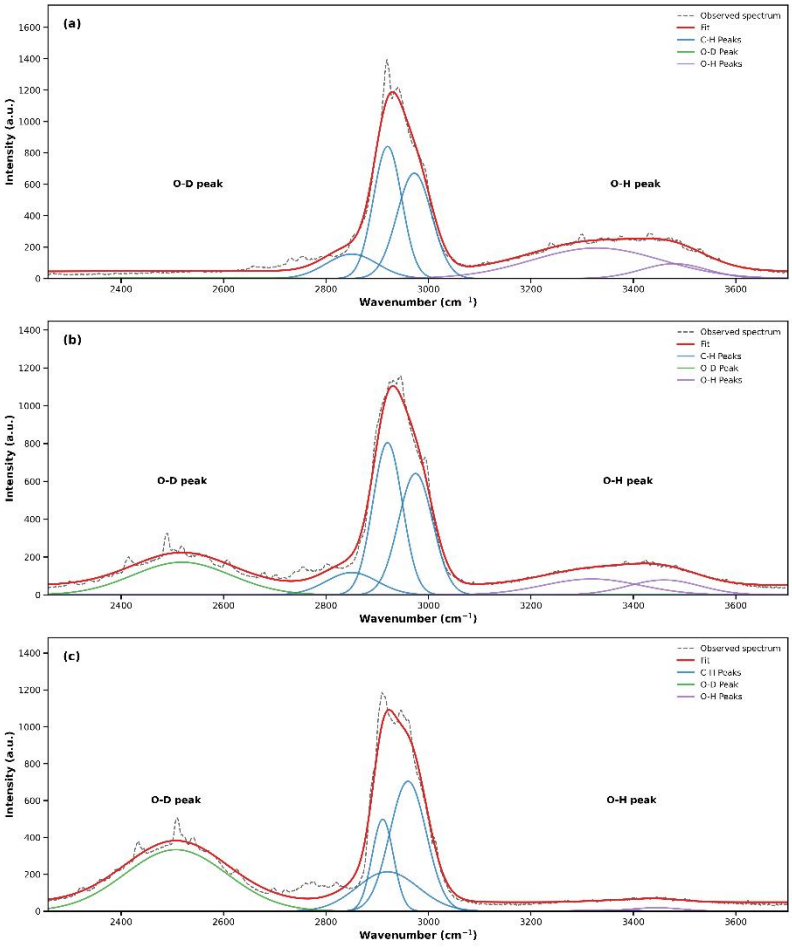

Figure 2: The Raman spectra of a sucrose droplet at RH=35% before D_2O exchange (a), during the exchange process (b), and after the exchange was completed (c). The grey dashed lines represent the measured Raman spectra. The green, blue, and purple lines denote the fitted O–D, C–H, and O–H bands, respectively, while the red lines represent the overall fitted spectra obtained by summing all fitted components.

3 Theoretical calculation of the D_2O fraction in an individual droplet

In isotope exchange experiments, the diffusion of D_2O within a droplet can be described by Fick's second law (Seinfeld and Pandis, 1998). In spherical coordinates, the diffusion equation can be written as

$$\frac{\partial C}{\partial t} = D_w \left[\frac{\partial^2 C}{\partial r^2} + \frac{2}{r}\frac{\partial C}{\partial r}\right], \quad (4)$$

where D_w is the diffusion coefficient of water within the droplet, and C denotes the D_2O concentration inside the droplet. This equation describes the evolution of the D_2O concentration in an individual droplet as a function of time and radial

https://doi.org/10.5194/egusphere-2026-3646
Preprint. Discussion started: 13 July 2026

position. Owing to the spherical symmetry of the model, a zero gradient condition must be satisfied at the droplet centre, namely,

$$(\frac{\partial C}{\partial r})_{r=0} = 0. \quad (5)$$

Meanwhile, during the diffusion of D_2O, the D_2O concentration at the droplet surface is assumed to remain constant:

$$C(R,t) = C_s, \quad (6)$$

where R is the droplet radius and C_s is the constant concentration at the droplet surface. Equations 5 and 6 are the boundary conditions that must be satisfied by the governing equation.

3.1 Initial condition in the diffusion model

In previous studies, the H_2O/D_2O exchange process has commonly been treated with the following initial condition: at the start of the model, the gas-phase D_2O concentration at the droplet surface is assumed to have instantaneously reached a stable value, while no D_2O is present within the droplet (Davies and Wilson, 2016; Nadler et al., 2019). Although this treatment facilitates an analytical solution, it does not fully reflect the actual experimental situation. In the experiment, after the H_2O-humidified gas stream is switched to the D_2O-humidified gas stream, the D_2O vapour concentration in the gas phase surrounding the droplet does not reach its steady value instantaneously, because replacing the original gas in the upstream tubing and sample cell takes a finite time. During this period, D_2O has already begun to diffuse from the droplet surface into the interior. Therefore, once the stable surface boundary condition has been established, the D_2O concentration within the droplet should no longer be assumed to be zero everywhere. If the idealised assumption of zero initial D_2O concentration in the droplet is retained, the retrieved diffusion coefficient will be affected by instrumental response during the initial stage of the experiment.

To better represent the experimental conditions, this study revises the initial condition while keeping the surface boundary condition unchanged and adopts a diffusion model with a non-uniform initial distribution. To describe this model in the simplest low-order form, the initial concentration profile is prescribed as a quadratic function of radius r, and the radially averaged fraction of D_2O within the droplet at t=0 is defined as Φ_0:

$$C(r,0) = Ar^2 + E, \quad (7)$$

$$\overline{C_0} = \frac{\int_0^R C(r,0)\,dr}{R} = \Phi_0 C_s. \quad (8)$$

Combined with the boundary condition at the droplet surface

$$C(R,0) = AR^2 + E = C_s, \quad (9)$$

the parameters in the initial concentration profile can be obtained as

$$A = \frac{3(1-\Phi_0)C_s}{2R^2}, \quad (10)$$

$$E = \frac{(3\Phi_0-1)C_s}{2}. \quad (11)$$

Accordingly, the initial condition adopted in this study can be written as

https://doi.org/10.5194/egusphere-2026-3646
Preprint. Discussion started: 13 July 2026

$$C(r,0) = \frac{3(1-\Phi_0)C_s}{2R^2}\cdot r^2 + \frac{(3\Phi_0-1)C_s}{2}. \quad (12)$$

3.2 D_2O concentration distribution in a droplet under non-uniform initial conditions

By combining the governing equation, the boundary conditions, and the initial condition, an analytical expression for the D_2O concentration distribution $C(r,t)$ in a droplet can be further derived. To homogenise the non-homogeneous boundary condition at the droplet surface, the following variable transformation is introduced:

$$v(r,t) = C(r,t) - C_s. \quad (13)$$

After this transformation, the diffusion equation, together with the corresponding initial and boundary conditions, can be written as

$$\frac{\partial v}{\partial t} = D_w\left[\frac{\partial^2 v}{\partial r^2} + \frac{2}{r}\frac{\partial v}{\partial r}\right], \quad (14)$$

$$v(r,0) = A(r^2 - R^2), \quad (15)$$

$$\left(\frac{\partial v}{\partial r}\right)_{r=0} = 0, \quad (16)$$

$$v(R,t) = 0. \quad (17)$$

Using the method of separation of variables, the general solution of the diffusion equation in spherical coordinates is obtained as

$$v(r,t) = \sum_{n=1}^{\infty} B_n \frac{sin(\frac{n\pi r}{R})}{r} exp(-\frac{n^2\pi^2 D_w t}{R^2}). \quad (18)$$

By applying the orthogonality of the eigenfunctions in the spherical coordinate system, the expansion coefficients B_n can be determined by integrating the initial condition $v(r,0)$:

$$B_n = \frac{2}{R}\int_0^R v(r,0)\frac{sin(\frac{n\pi r}{R})}{r}\cdot r^2 dr. \quad (19)$$

Finally, the concentration distribution $C(r,t)$ can be expressed as:

$$\frac{C(r,t)}{C_s} = 1 + \frac{R}{r}\sum_{n=1}^{\infty}\frac{18(1-\Phi_0)(-1)^n}{n^3\pi^3} sin(\frac{n\pi r}{R}) exp(-\frac{n^2\pi^2 D_w t}{R^2}). \quad (20)$$

Detailed derivation of Eq. (20) is provided in the Supplement.

3.3 Radially averaged D_2O concentration in a droplet

In Sect. 3.2, the concentration distribution of D_2O in a droplet was obtained. On this basis, the average D_2O concentration in a droplet can be further evaluated. As noted above, in an optical tweezers system, the concentration signal derived from Raman spectroscopy is more appropriately represented by the radially averaged concentration within the droplet. On this basis, the theoretical concentration distribution is radially averaged in the present study to describe the temporal evolution of the D_2O concentration in a droplet and to establish correspondence with the Raman signal measured in the experiment:

$$\Phi_{D_2O}(t) = \frac{\overline{C(t)}}{C_s} = \frac{1}{C_s}\frac{1}{R}\int_0^R C(r,t)\, dr. \quad (21)$$

https://doi.org/10.5194/egusphere-2026-3646
Preprint. Discussion started: 13 July 2026

where $\overline{C(t)}$ is the radially averaged concentration of D_2O in the droplet, and $\Phi_{D_2O}(t)$ represents the temporal evolution of the radially averaged D_2O fraction within the droplet. By substituting the expression for $C(r,t)$ into the integral and carrying out the integration, the expression for $\Phi_{D_2O}(t)$ is obtained:

$$\Phi_{D_2O}(t) = 1 + \sum_{n=1}^{\infty} \frac{18(1-\Phi_0)(-1)^n}{n^3\pi^3} Si(n\pi) exp(-\frac{n^2\pi^2 D_w t}{R^2}). \quad (22)$$

where $Si(n\pi)$ denotes the value of the sine integral function evaluated at $n\pi$. Detailed derivation of Eq. (22) is provided in the Supplement. For simplicity, the series term is denoted by Sn, and $\Phi_{D_2O}(t)$ can then be written as

$$\Phi_{D_2O}(t) = 1 + \sum_{n=1}^{\infty} S_n exp(-\frac{n^2\pi^2 D_w t}{R^2}), \quad (23)$$

$$S_n = \frac{18(1-\Phi_0)(-1)^n}{n^3\pi^3} Si(n\pi). \quad (24)$$

This relationship is then used to determine the water diffusion coefficient from the Raman spectroscopic data.

4 New method for determining the water diffusion coefficient in an individual droplet based on the diffusion characteristic time

In this study, we propose a method for retrieving the water diffusion coefficient D_w in a droplet from the characteristic time of D_2O diffusion. In contrast to conventional fitting-based approaches, which obtain D_w by fitting the measured time series of the D_2O fraction to the theoretical expression, this method determines D_w directly from the quantitative relationship between the characteristic time and the diffusion coefficient.

4.1 Characteristic time of D_2O diffusion in the droplet

The temporal evolution of the D_2O fraction in a droplet is described by Eq. (22), in which the time-dependent term contains a series of exponential decay factors $exp(-\frac{n^2\pi^2 D_w t}{R^2})$. The characteristic time τ is defined from the first term in the exponential (Seinfeld and Pandis, 1998) and is

$$\tau = \frac{R^2}{\pi^2 D_w}. \quad (25)$$

The characteristic time reflects the timescale of D_2O redistribution within the droplet. For a given droplet radius, a shorter characteristic time corresponds to faster diffusion and a larger water diffusion coefficient, whereas a longer characteristic time indicates slower diffusion. The water diffusion coefficient can therefore be calculated from the characteristic time as follows:

$$D_w = \frac{R^2}{\pi^2 \tau}. \quad (26)$$

4.2 D_2O fraction corresponding to the characteristic time

At the initial time, the initial D_2O fraction within the droplet is:

https://doi.org/10.5194/egusphere-2026-3646
Preprint. Discussion started: 13 July 2026

$$\Phi_{D_2O}(0) = \Phi_0. \quad (27)$$

When $t = \tau$, that is, when diffusion has proceeded to the time corresponding to the characteristic time, the D_2O fraction within the droplet can be expressed as

$$\Phi_{D_2O}(\tau) = 1 + \sum_{n=1}^{\infty} S_n exp(-n^2). \quad (28)$$

Table 1 lists the numerical contributions of the first few terms in the series of $\Phi_{D_2O}(\tau)$. It can be seen that the contribution of each term decreases rapidly with increasing n; when n=3, the contribution of the series term to $\Phi_{D_2O}(\tau)$ is already negligible. Therefore, under the condition $t = \tau$, $\Phi_{D_2O}(\tau)$ can be approximated by the first two terms as

$$\Phi_{D_2O}(\tau) = 0.6064 + 0.3936\Phi_0. \quad (29)$$

Therefore, the value of $\Phi_{D_2O}(\tau)$ is uniquely determined by the initial fraction Φ_0. This means that, once the initial D_2O fraction is known, the D_2O fraction corresponding to the characteristic time can be calculated from Eq. (29). The characteristic time can then be identified from the experimental curve as the time required for the D_2O fraction to increase from Φ_0 to the theoretically predicted value $\Phi_{D_2O}(\tau)$. Finally, based on the relationship between the characteristic time and the diffusion coefficient given by Eq. (26), the water diffusion coefficient in a droplet can be further determined.

Table 1: Numerical values of the terms in $\Phi_{D_2O}(\tau)$ for different values of n.

n	$exp(-n^2)$	S_n	$S_n exp(-n^2)$
1	0.3679	$-1.0751(1-\Phi_0)$	$-0.3955(1-\Phi_0)$
2	0.0183	$0.10291(1-\Phi_0)$	$0.0019(1-\Phi_0)$
3	0.0001	$-0.0360(1-\Phi_0)$	≈ 0

4.3 Determination of the experimental initial time

Because the method proposed in this study requires the initial D_2O fraction to be determined first, identifying the experimental initial time is critical. In the diffusion model described above, the D_2O vapour concentration at the droplet surface is approximated as a stable boundary value. The starting point in the experiment is therefore defined as the moment when this surface boundary condition is established, that is, when the external D_2O vapour concentration becomes stable. In the present experiment, this moment was identified from the stabilisation of the relative humidity signal. The initial D_2O fraction in the droplet was then defined as the value measured at this starting point.

Given the response characteristics of the RH probe, once the RH approaches steady state, the measured RH data, shown as blue points in Fig. 3, typically exhibit small variations around a stable value. To determine the time at which RH reaches a stable state more accurately, an exponential function was used to fit the temporal evolution of RH, where α, β, and ω are fitting parameters:

$$RH = \alpha e^{-\frac{t}{\omega}} + \beta. \quad (30)$$

https://doi.org/10.5194/egusphere-2026-3646
Preprint. Discussion started: 13 July 2026

Considering that an exponential process is sufficiently close to its steady-state value after approximately five characteristic times, the RH stabilisation time, t_{stable}, was defined here as five times the characteristic time of the fitted function:

$$t_{stable} = 5\omega. \quad (31)$$

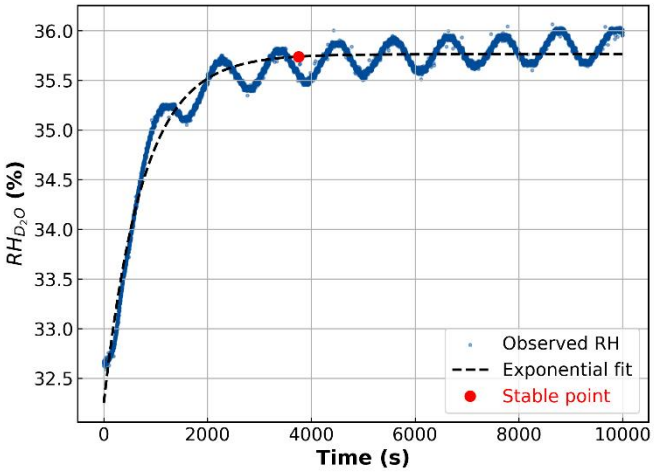

Figure 3: Temporal variation of RH and the corresponding exponential fit in a representative experiment. The blue points denote the measured RH data, the dashed line denotes the exponential fitting curve, and the red point marks the time at which RH reaches a stable value.

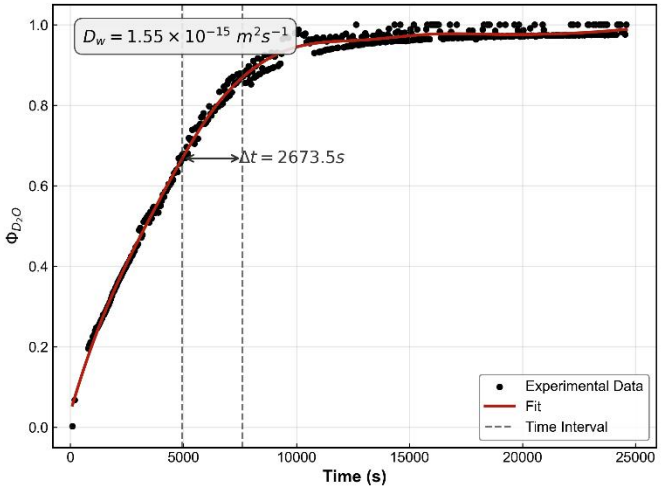

Figure 4: Temporal evolution of the D_2O fraction in a representative experiment. The two dashed lines represent the time at which RH reaches a stable value and the time at which the D_2O fraction reaches the theoretically predicted value at the characteristic time. The interval between these two time points is the characteristic time.

In Fig. 3, the dashed line denotes the fitting curve, and the red marker indicates the RH stabilisation time for an example experiment in which the stabilised RH was approximately 35.5%. It should be noted that the time origin (t=0) in Fig. 3 corresponds to the minimum point of this RH variation curve, rather than the actual onset of D_2O flow switching, in order to improve the accuracy of the exponential fit. The time interval between initiation of the D_2O flow switching and RH

https://doi.org/10.5194/egusphere-2026-3646
Preprint. Discussion started: 13 July 2026

stabilisation in this experiment was approximately 4956 s. Figure 4 shows the temporal evolution of the D_2O fraction derived from the Raman spectral changes in the same experiment. The two dashed lines in Fig. 4 mark the time at which RH reaches a stable value and the time at which the D_2O fraction reaches the theoretically predicted value at the characteristic time. The interval between these two time points corresponds to the characteristic time, from which the water diffusion coefficient was determined to be 1.55×10^{-15} m^2s^{-1}.

5 Results and Discussion

5.1 Measured water diffusion coefficients in sucrose droplets at different RH

In this study, a characteristic-time-based method was implemented in an optical tweezers system to determine the diffusion coefficient of water in individual sucrose droplets under different relative humidity conditions. The results show that, over the RH range of 30–45%, the diffusion coefficient of water in sucrose droplets is on the order of 1×10^{-16}–1×10^{-14} m^2s^{-1} (Fig. 5). As RH decreases, D_w exhibits an overall decline. This trend indicates that water loss under drier conditions increases the sucrose concentration in the droplet and reduces the bulk-phase diffusivity, while internal mass transport slows. The uncertainty in D_w was evaluated by considering the combined effects of uncertainties associated with Raman spectral fitting, droplet radius determination, possible differences in the diffusion behaviour of H_2O and D_2O, and variations in ambient temperature and relative humidity during the experiments (Reid et al., 2007; Mills, 1973; Davies and Wilson, 2016; Nadler et al., 2019). On this basis, the resulting relative uncertainty in D_w was estimated to be 50%. The absolute RH uncertainty was approximately ±2% RH, mainly reflecting the precision of the humidity probe and variations in environmental conditions.

To further characterise the composition dependence of the water diffusion coefficient, the experimental results were fit to a Vignes-type parameterisation. This empirical formulation is commonly used for binary liquid mixtures, in which the logarithm of the diffusion coefficient is assumed to vary approximately linearly with composition in a weighted manner, rather than the diffusion coefficient itself following a simple linear dependence (Vignes, 1966):

$$\ln(D_w) = \alpha x_w \ln(D^0_{w,w}) + (1-\alpha x_w)\ln(D^0_{w,s}), \quad (32)$$

where $D^0_{w,w}$ denotes the diffusion coefficient of water in pure water (2×10^{-9} m^2s^{-1}), $D^0_{w,s}$ is the diffusion coefficient of water in the pure solute, x_w is the mole fraction of water, D_w is the diffusion coefficient of water in the solution at the given composition, and α is an empirical parameter introduced to account for non-ideal effects in the system. The calculations of α and x_w were based on the empirical expressions reported by previous research (Norrish, 1966; Davies and Wilson, 2016).

Figure 5 presents the measured water diffusion coefficients together with the fitted Vignes-type parameterisation. The measured D_w values decrease with decreasing RH and are well described by the Vignes-type parameterisation, suggesting that the composition dependence of water diffusion in sucrose droplets is reasonably represented. These results were further compared with previously reported values (Zobrist et al., 2011; Price et al., 2014; Davies and Wilson, 2016). The

https://doi.org/10.5194/egusphere-2026-3646
Preprint. Discussion started: 13 July 2026

comparison shows that the diffusion coefficients obtained in this study are broadly consistent with previous experimental results in both overall trend and order of magnitude. This consistency is particularly clear for Raman isotope-tracing studies. Although those studies used different experimental platforms, including electrodynamic balance (EDB) and solution-disk diffusion systems, the reported D_w values are comparable to those obtained here. The minor differences among these Raman isotope-tracing studies may be related to differences in experimental platforms, instrumental performance, and environmental control. This agreement indicates that the experimental measurements and retrieval procedure used in this study can reasonably characterise the diffusion behaviour of water in sucrose droplets. At RH below approximately 30%, however, the results reported by Zobrist et al. differ from those obtained in the present study and from those reported in other Raman isotope-tracing studies, with their estimated diffusion coefficients being approximately one to two orders of magnitude higher than the values reported here (Zobrist et al., 2011). Previous studies have suggested that this discrepancy mainly arises from differences in how the two types of methods treat droplet mass transport and boundary conditions (Nadler et al., 2019). Zobrist et al. derived diffusion coefficients using a mass transfer model based on droplet evaporation and hygroscopic growth, whereas the Raman isotope tracer method is based on a diffusion model that assumes a constant droplet radius and a stable external gas-phase concentration(Zobrist et al., 2011; Davies and Wilson, 2016; Nadler et al., 2019). These different assumptions can lead to pronounced discrepancies under low-RH conditions.

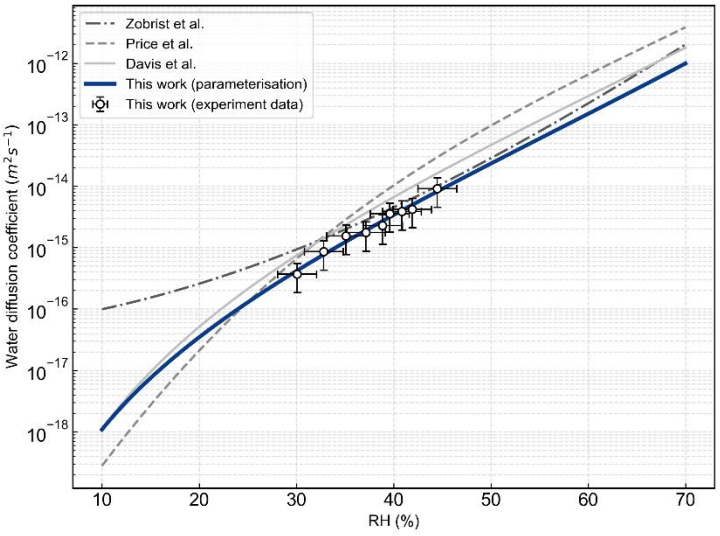

Figure 5: Measured water diffusion coefficients in sucrose droplets at different RH in this study and comparison with parameterisations reported by Zobrist et al., Price et al., and Davies et al (Zobrist et al., 2011; Price et al., 2014; Davies and Wilson, 2016).

5.2 Advantages of the characteristic-time-based method for measuring water diffusion coefficients

Compared with conventional approaches that determine D_w by fitting the complete time series of the D_2O fraction, the characteristic-time-based method developed in this study reduces the required observation time, simplifies data processing, and enhances the feasibility of measurements in slow diffusion systems.

https://doi.org/10.5194/egusphere-2026-3646
Preprint. Discussion started: 13 July 2026

In this method, the temporal evolution of the D_2O fraction within the droplet is obtained from Raman spectra. The characteristic time is then determined as the time at which the measured D_2O fraction reaches the value predicted by the diffusion model, and the water diffusion coefficient is subsequently determined from the relationship between characteristic time and diffusion coefficient. Therefore, the method developed in this study does not require the complete H_2O/D_2O exchange process to be tracked. The determination of the water diffusion coefficient only requires the D_2O fraction data from the initial time to the characteristic time. This feature substantially reduces the required observation time, making the method more suitable for measurements in slow diffusion systems. As discussed in Sect. 1, when internal mass transport is strongly hindered, measurements at a given RH can require a long experimental duration. The present method therefore provides a useful technical approach for investigating water diffusion under more challenging conditions, such as low temperature and low relative humidity.

The method developed in this study can also be extended to diffusion systems with different initial concentration distributions, definitions of the averaged internal D_2O fraction, and system geometries. In this work, a spherically symmetric diffusion model with a non-uniform initial condition was established based on Fick's second law. It should be noted that, for spherical droplets with the governing equation and boundary conditions fixed, different initial distributions yield distinct expressions for the concentration distribution inside the droplet. In addition, the averaging method used to calculate the internal D_2O fraction from these concentration distributions, such as volume averaging or radial averaging, will also affect the specific form of the resulting internal D_2O fraction, denoted here as $\Phi_{D_2O}(t)$. However, these differences are mainly reflected in the expansion coefficients of $\Phi_{D_2O}(t)$, whereas the fundamental structure of the temporal decay terms is generally preserved, namely:

$$\Phi_{D_2O}(t) = 1 + \sum_{n=1}^{\infty} T_n exp\left(-\frac{n^2\pi^2 D_w t}{R^2}\right), \quad (33)$$

where T_n is the expansion coefficients. Taking the case commonly considered in previous studies as an example (Nadler et al., 2019), when the initial D_2O fraction within the droplet is zero, and the internal D_2O fraction is defined based on volume averaging, the expression of $\Phi_{D_2O}(t)$ can be written as:

$$\Phi_{D_2O}(t) = 1 - \frac{6}{\pi^2}\sum_{n=1}^{\infty} \frac{1}{n^2} exp\left(-\frac{n^2\pi^2 D_w t}{R^2}\right). \quad (34)$$

This shows that the characteristic-time-based method for determining diffusion coefficients is not limited to the non-uniform initial condition adopted in this study. For spherical droplets, once the theoretical expression for $\Phi_{D_2O}(t)$ is re-derived under the given conditions, the characteristic time can be determined following the same procedure, from which the diffusion coefficient can then be derived. Furthermore, for diffusion systems with other geometries, such as solution disks, although the geometry is no longer spherical and the corresponding expression for the time evolution of the concentration distributions changes accordingly, the solution to such problems can still generally be written as a series expansion in terms of eigenfunctions, with the time-dependent terms retaining an exponential decay structure (Price et al., 2014). This indicates that such systems also have a characteristic time that can be used to characterise the diffusion process and to determine diffusion coefficients. Overall, the characteristic-time-based method is not restricted to the condition employed in this study.

https://doi.org/10.5194/egusphere-2026-3646
Preprint. Discussion started: 13 July 2026

Rather, it can be adapted to the specific geometry and initial state of a given diffusion system, thereby providing an effective approach for diffusion studies across different experimental platforms.

6 Conclusions

In this study, a new characteristic-time-based method was developed for the direct determination of the water diffusion coefficient in an individual highly viscous droplet by tracing H_2O/D_2O exchange using Raman spectroscopy. Using this method, we measured the diffusion coefficients of water in sucrose droplets at relative humidities of 30–45%. The results are generally consistent with previous studies in both trend and order of magnitude, and also agree with the composition dependence described by the Vignes-type parameterisation, confirming the validity of the method.

This method provides a new analytical approach for directly measuring the water diffusion coefficient. Compared with conventional methods that rely on fitting the entire time series of H_2O/D_2O exchange, this method requires only data describing droplet evolution from the initial state to the state corresponding to the characteristic time, thereby reducing the experimental observation time. Moreover, this method is not limited to the spherical model and non-uniform initial condition adopted in this study, but can be adapted to diffusion systems with different geometries and initial states. In such systems, a characteristic time that characterises the diffusion process can generally be identified, allowing the same principle to be used to determine water diffusion coefficients. The method can therefore be applied to measurements of water diffusion coefficients in highly viscous systems on different experimental platforms and under more complex conditions, such as low temperature and low relative humidity. This broader applicability will support further studies of aerosol phase state, mass transfer, and related atmospheric chemical processes in highly viscous aerosol particles.

Code and data availability

Codes used in this study are available on request from the corresponding author (email: zcs@pku.edu.cn). The data presented in the study can be found at https://disk.pku.edu.cn/link/AADABD319766AC45F99DA10C93BAAFA0AA.

Author contribution

S.G. proposed the idea, conducted the experiments, analysed the data, and wrote the manuscript. C.F. contributed to the discussion. C.Z. contributed to the discussion and reviewed and revised the manuscript.

Competing interests

The contact author has declared that none of the authors has any competing interests.

https://doi.org/10.5194/egusphere-2026-3646
Preprint. Discussion started: 13 July 2026

Disclaimer

Copernicus Publications remains neutral with regard to jurisdictional claims made in the text, published maps, institutional affiliations, or any other geographical representation in this paper. While Copernicus Publications makes every effort to include appropriate place names, the final responsibility lies with the authors. Views expressed in the text are those of the authors and do not necessarily reflect the views of the publisher.

Acknowledgements

We sincerely acknowledge financial support from the National Natural Science Foundation of China (42530602 and 42275070) and technical assistance from Cai Chen. During the preparation of an early version of this manuscript, the authors used ChatGPT for language polishing. After using this tool, the authors carefully reviewed and revised the content and take full responsibility for the published material.

Financial support

This work is supported by the National Natural Science Foundation of China (42530602 and 42275070).

References

Davies, J. F. and Wilson, K. R.: Raman Spectroscopy of Isotopic Water Diffusion in Ultraviscous, Glassy, and Gel States in Aerosol by Use of Optical Tweezers, Anal. Chem., 88, 2361–2366, https://doi.org/10.1021/acs.analchem.5b04315, 2016.

Evoy, E., Maclean, A. M., Rovelli, G., Li, Y., Tsimpidi, A. P., Karydis, V. A., Kamal, S., Lelieveld, J., Shiraiwa, M., Reid, J. P., and Bertram, A. K.: Predictions of diffusion rates of large organic molecules in secondary organic aerosols using the Stokes–Einstein and fractional Stokes–Einstein relations, Atmos. Chem. Phys., 19, 10073–10085, https://doi.org/10.5194/acp-19-10073-2019, 2019.

Fan, C., He, B., Guo, S., Qiu, J., and Zhao, C.: Insights into the real part of natural sea spray aerosol refractive index in the Pacific Ocean, Atmos. Chem. Phys., 25, 5761–5771, https://doi.org/10.5194/acp-25-5761-2025, 2025.

Gou, Y., Xie, M., and Chen, J.: The phase state and viscosity of organic aerosol and related impacts on atmospheric physicochemical processes: A review, Atmospheric Environment, 343, 120985, https://doi.org/10.1016/j.atmosenv.2024.120985, 2025.

Hosny, N. A., Fitzgerald, C., Tong, C., Kalberer, M., Kuimova, M. K., and Pope, F. D.: Fluorescent lifetime imaging of atmospheric aerosols: a direct probe of aerosol viscosity, Faraday Discuss., 165, 343, https://doi.org/10.1039/c3fd00041a, 2013.

Hosny, N. A., Fitzgerald, C., Vyšniauskas, A., Athanasiadis, A., Berkemeier, T., Uygur, N., Pöschl, U., Shiraiwa, M., Kalberer, M., Pope, F. D., and Kuimova, M. K.: Direct imaging of changes in aerosol particle viscosity upon hydration and chemical aging, Chem. Sci., 7, 1357–1367, https://doi.org/10.1039/C5SC02959G, 2016.

https://doi.org/10.5194/egusphere-2026-3646
Preprint. Discussion started: 13 July 2026

Kiland, K. J., Marroquin, K. L., Smith, N. R., Xu, S., Nizkorodov, S. A., and Bertram, A. K.: A new hot-stage microscopy technique for measuring temperature-dependent viscosities of aerosol particles and its application to farnesene secondary organic aerosol, Atmos. Meas. Tech., 15, 5545–5561, https://doi.org/10.5194/amt-15-5545-2022, 2022.

Madawala, C. K., Lee, H. D., Kaluarachchi, C. P., and Tivanski, A. V.: Quantifying the Viscosity of Individual Submicrometer Semisolid Particles Using Atomic Force Microscopy, Anal. Chem., 95, 14566–14572, https://doi.org/10.1021/acs.analchem.3c01835, 2023.

Mason, B. J.: The physics of clouds, Second edition, first published in paperback., Oxford Univ. Press, Oxford, 671 pp., 2010.

Mills, R.: Self-diffusion in normal and heavy water in the range 1-45.deg., J. Phys. Chem., 77, 685–688, https://doi.org/10.1021/j100624a025, 1973.

Nadler, K. A., Kim, P., Huang, D.-L., Xiong, W., and Continetti, R. E.: Water diffusion measurements of single charged aerosols using H_2 O/D_2 O isotope exchange and Raman spectroscopy in an electrodynamic balance, Phys. Chem. Chem. Phys., 21, 15062–15071, https://doi.org/10.1039/C8CP07052K, 2019.

Narten, A.: Thermodynamic Effects of Mixing Light and Heavy Water, The Journal of Chemical Physics, 41, 1318–1321, https://doi.org/10.1063/1.1726066, 1964.

Norrish, R. S.: An equation for the activity coefficients and equilibrium relative humidities of water in confectionery syrups, Int J of Food Sci Tech, 1, 25–39, https://doi.org/10.1111/j.1365-2621.1966.tb01027.x, 1966.

Power, R. M., Simpson, S. H., Reid, J. P., and Hudson, A. J.: The transition from liquid to solid-like behaviour in ultrahigh viscosity aerosol particles, Chem. Sci., 4, 2597, https://doi.org/10.1039/c3sc50682g, 2013.

Price, H. C., Murray, B. J., Mattsson, J., O'Sullivan, D., Wilson, T. W., Baustian, K. J., and Benning, L. G.: Quantifying water diffusion in high-viscosity and glassy aqueous solutions using a Raman isotope tracer method, Atmos. Chem. Phys., 14, 3817–3830, https://doi.org/10.5194/acp-14-3817-2014, 2014.

Qiu, J., He, B., Zhang, L., Cheng, M., Guo, S., Fan, C., and Zhao, C.: Hygroscopic behavior of sea spray aerosols in offshore waters and open sea areas investigated with aerosol optical tweezers, Atmospheric Environment, 321, 120360, https://doi.org/10.1016/j.atmosenv.2024.120360, 2024.

Rasool, Q. Z., Shrivastava, M., Liu, Y., Gaudet, B., and Zhao, B.: Modeling the Impact of the Organic Aerosol Phase State on Multiphase OH Reactive Uptake Kinetics and the Resultant Heterogeneous Oxidation Timescale of Organic Aerosol in the Amazon Rainforest, ACS Earth Space Chem., 7, 1009–1024, https://doi.org/10.1021/acsearthspacechem.2c00366, 2023.

Reid, J. P., Meresman, H., Mitchem, L., and Symes†, R.: Spectroscopic studies of the size and composition of single aerosol droplets, International Reviews in Physical Chemistry, 26, 139–192, https://doi.org/10.1080/01442350601081899, 2007.

Reid, J. P., Bertram, A. K., Topping, D. O., Laskin, A., Martin, S. T., Petters, M. D., Pope, F. D., and Rovelli, G.: The viscosity of atmospherically relevant organic particles, Nat Commun, 9, 956, https://doi.org/10.1038/s41467-018-03027-z, 2018.

Renbaum-Wolff, L., Grayson, J. W., Bateman, A. P., Kuwata, M., Sellier, M., Murray, B. J., Shilling, J. E., Martin, S. T., and Bertram, A. K.: Viscosity of α -pinene secondary organic material and implications for particle growth and reactivity, Proc. Natl. Acad. Sci. U.S.A., 110, 8014–8019, https://doi.org/10.1073/pnas.1219548110, 2013.

https://doi.org/10.5194/egusphere-2026-3646
Preprint. Discussion started: 13 July 2026

Seinfeld, J. H. and Pandis, S. N.: Atmospheric chemistry and physics: from air pollution to climate change, Wiley, New York, 1998.

Semeniuk, K. and Dastoor, A.: Current State of Atmospheric Aerosol Thermodynamics and Mass Transfer Modeling: A Review, Atmosphere, 11, 156, https://doi.org/10.3390/atmos11020156, 2020.

Shiraiwa, M. and Seinfeld, J. H.: Equilibration timescale of atmospheric secondary organic aerosol partitioning, Geophysical Research Letters, 39, 2012GL054008, https://doi.org/10.1029/2012GL054008, 2012.

Shiraiwa, M., Li, Y., Tsimpidi, A. P., Karydis, V. A., Berkemeier, T., Pandis, S. N., Lelieveld, J., Koop, T., and Pöschl, U.: Global distribution of particle phase state in atmospheric secondary organic aerosols, Nat Commun, 8, 15002, https://doi.org/10.1038/ncomms15002, 2017.

Slade, J. H. and Knopf, D. A.: Multiphase OH oxidation kinetics of organic aerosol: The role of particle phase state and relative humidity, Geophysical Research Letters, 41, 5297–5306, https://doi.org/10.1002/2014GL060582, 2014.

Song, Y.-C., Ingram, S., Arbon, R. E., Topping, D. O., Glowacki, D. R., and Reid, J. P.: Transient cavity dynamics and divergence from the Stokes–Einstein equation in organic aerosol, Chem. Sci., 11, 2999–3006, https://doi.org/10.1039/C9SC06228A, 2020.

Vignes, A.: Diffusion in Binary Solutions. Variation of Diffusion Coefficient with Composition, Ind. Eng. Chem. Fund., 5, 189–199, https://doi.org/10.1021/i160018a007, 1966.

Virtanen, A., Joutsensaari, J., Koop, T., Kannosto, J., Yli-Pirilä, P., Leskinen, J., Mäkelä, J. M., Holopainen, J. K., Pöschl, U., Kulmala, M., Worsnop, D. R., and Laaksonen, A.: An amorphous solid state of biogenic secondary organic aerosol particles, Nature, 467, 824–827, https://doi.org/10.1038/nature09455, 2010.

Wilson, T. W., Murray, B. J., Wagner, R., Möhler, O., Saathoff, H., Schnaiter, M., Skrotzki, J., Price, H. C., Malkin, T. L., Dobbie, S., and Al-Jumur, S. M. R. K.: Glassy aerosols with a range of compositions nucleate ice heterogeneously at cirrus temperatures, Atmos. Chem. Phys., 12, 8611–8632, https://doi.org/10.5194/acp-12-8611-2012, 2012.

Zaveri, R. A., Shilling, J. E., Zelenyuk, A., Liu, J., Bell, D. M., D'Ambro, E. L., Gaston, C. J., Thornton, J. A., Laskin, A., Lin, P., Wilson, J., Easter, R. C., Wang, J., Bertram, A. K., Martin, S. T., Seinfeld, J. H., and Worsnop, D. R.: Growth Kinetics and Size Distribution Dynamics of Viscous Secondary Organic Aerosol, Environ. Sci. Technol., 52, 1191–1199, https://doi.org/10.1021/acs.est.7b04623, 2018.

Zhou, S., Shiraiwa, M., McWhinney, R. D., Pöschl, U., and Abbatt, J. P. D.: Kinetic limitations in gas-particle reactions arising from slow diffusion in secondary organic aerosol, Faraday Discuss., 165, 391–406, https://doi.org/10.1039/C3FD00030C, 2013.

Zobrist, B., Marcolli, C., Pedernera, D. A., and Koop, T.: Do atmospheric aerosols form glasses?, Atmos. Chem. Phys., 8, 5221–5244, https://doi.org/10.5194/acp-8-5221-2008, 2008.

Zobrist, B., Soonsin, V., Luo, B. P., Krieger, U. K., Marcolli, C., Peter, T., and Koop, T.: Ultra-slow water diffusion in aqueous sucrose glasses, Phys. Chem. Chem. Phys., 13, 3514, https://doi.org/10.1039/c0cp01273d, 2011.